Symmetric mass fragmentation following capture in reactions of 4.8—8 MeV/nucleon ^{208}Pb on ^{50}Ti, ^{52}Cr, ^{58}Fe, and ^{64}Ni using the fusion model based on the dynamical fragmentation theory

R. Aroumougame, N. Malhotra, S. S. Malik, and Raj K. Gupta

Physics Department, Panjab University, Chandigarh-160014, India

(Received 10 July 1986)

As a first application of our fusion model, the dynamical fragmentation process of fusion and subsequent fission is analyzed in the reactions of 4.8—8 MeV/nucleon ^{208}Pb on ^{50}Ti, ^{52}Cr, ^{58}Fe, and ^{64}Ni. In this two step model, the colliding nuclei are first shown to be captured in the pockets behind the adiabatic interaction barriers and then the composite systems so formed, being strongly excited, fission adiabatically. The calculated capture cross sections agree reasonably well with the experiments and the mass distributions are systematically symmetric, independent of the choice of relative separation distance R and the large structure in the cranking masses. The symmetric mass fragmentation is a (dynamical) liquid drop effect and the peaks or other detailed structure in mass distributions depend on how the temperature would modify the masses and also on the dynamical coupling of mass asymmetry with the relative motion. This demands refined measurements of the fission data for larger mass asymmetry. The calculated critical angular momentum, which refers to the vanishing of the interaction barrier, in these reactions occurs at the incident energy greater than 8 MeV/nucleon. This suggests a possible importance of extending these experiments beyond their present energy limits.

I. INTRODUCTION

In reactions of 4.8—8 MeV/nucleon ^{208}Pb beam bombarded on many light targets of ^{26}Mg, ^{27}Al, ^{48}Ca, ^{50}Ti, ^{52}Cr, ^{58}Fe, and ^{64}Ni, recently the cross sections for making the fused systems are measured (called the capture cross sections) and the fused systems are then found to disintegrate with fragment mass distributions centered around zero mass asymmetry.[1] The measured excitation energies are also large—about 70—80% of the Coulomb barrier heights at 8 MeV/nucleon. This process of capture and subsequent symmetric mass fragmentation observed in these reactions is in contrast to the other deep inelastic collisions where the mass distribution is peaked around the entrance channel (called the quasi-fission reactions).[2]

In this paper we show that the above mentioned two step process of "symmetric mass fragmentation following capture" is given satisfactorily within the fusion model of our earlier paper[3] (hereafter referred to as I), based on the dynamical fragmentation theory. The fused or the captured system in this model is formed by the crossing over of an adiabatic interaction barrier and, depending on the excitation energy, which is shown to increase as mass asymmetry increases, the captured system proceeds to form a cool compound nucleus or the fusion-fission process occurs. Since the partners involved in the reactions studied here have all very large mass asymmetries, the second possibility of fusion-fission is expected to happen such that the symmetric mass fragmentation is given by the adiabatic fission of the excited composite system formed.

The process of capture and subsequent symmetric fragmentation is also given by the three-dimensional time-dependent Hartree-Fock calculations of Stöcker *et al.*[4]

Also, Swiatecki[5] has proposed a similar two-step model of "nuclear coalescence and reseparation" for these reactions. Within the fragmentation theory, a two-step model of "fission following a few-nucleon transfer" was applied much earlier by one of us,[6] very successfully, to quasi-fission reactions.

A very brief description of the theory is given in Sec. II and we use it first to calculate the angular momentum dependent adiabatic scattering potentials, in Sec. III. Calculations of the first step (the capture cross sections) and the second step (mass distribution yields) of our model are presented in Secs. IV and V, respectively. Our conclusions are summarized in Sec. VI.

II. THE DYNAMICAL FRAGMENTATION THEORY

Using the coordinates of relative separation R (or, equivalently, the length coordinate $\lambda = l/2R_0$, with l the total length of the system and R_0 the radius of the corresponding spherical nucleus), the deformations β_i ($i = 1,2$), the neck parameter ϵ (see Fig. 15), the mass asymmetry $\eta = (A_1 - A_2)/(A_1 + A_2)$, and the charge asymmetry $\eta_Z = (Z_1 - Z_2)/(Z_1 + Z_2)$, the collective Hamiltonian of the fragmentation theory[7] is written as

$$H = T(\mathbf{R},\beta_i,\eta,\eta_Z;\dot{\mathbf{R}},\dot{\beta_i},\dot{\eta},\dot{\eta}_Z) + V(\mathbf{R},\beta_i,\eta,\eta_Z) \,, \tag{1}$$

where the collective potential V is calculated using the Strutinsky method from the asymmetric two center shell model[8] (ATCSM) and the appropriate liquid drop model[9] (LDM). For $R < R_1 + R_2$, the adiabatic potentials are obtained by carrying out three dimensional minimization in shape parameters β_i and ϵ and, for $R \geq R_1 + R_2$, the potential can be expressed simply as

$$V(R,\eta) = -B_1(A_1, Z_1) - B_2(A_2, Z_2) + E_C + V_P + V_l \ . \quad (2)$$

Here, A_i, Z_i are fixed by minimizing in the charge asymmetry η_Z, the sum of the two binding energies $B_i(A_i, Z_i)$ (taken from Seeger[10] and the 1983 compilation of the IAEA, Vienna). The Coulomb interaction E_C and the proximity potential V_P are calculated as described in paper I. For the angular momentum contribution, we have

$$V_l = \frac{\hbar^2}{2\mathscr{I}_\perp} l(l+1) \ , \quad (3)$$

where, in terms of the bombarding center-of-mass energy $E_{c.m.}$,

$$l = \frac{R\sqrt{2\mu E_{c.m.}}}{\hbar} \ , \quad (4)$$

with

$$\mu = \frac{A_1 A_2}{A_1 + A_2} m = \tfrac{1}{4} A m (1 - \eta^2) \quad (5)$$

as the reduced mass. m is the nucleon mass. $\mathscr{I}_\perp$ is the moment of inertia of the rotating system about an axis perpendicular to the symmetry axis, which for the overlap region $(R < R_1 + R_2)$ is given by Eq. (A5), derived in the Appendix for the ATCSM nuclear shape. (For a two center shell model nuclear shape, the moment of inertia about the symmetry axis itself, $\mathscr{I}_{||}$, is also derived in the Appendix.) For $R = R_1 + R_2$, one can use the complete sticking limit, such that

$$\mathscr{I}_\perp = \mu R^2 + \tfrac{2}{5} A_1 m R_1^2 + \tfrac{2}{5} A_2 m R_2^2 \ , \quad (6)$$

which, for the separated nuclei $(R > R_1 + R_2)$, becomes simply equal to μR^2, the so-called nonsticking limit.

The mass parameters B_{ij} for the kinetic energy term are consistently calculated by using the ATCSM states in the adiabatic cranking formula based on the BCS formalism (see Refs. 7 and 11 for details).

The temperature effects on the potential are brought in here through the well accepted relation[12]

$$V = V_{\text{LDM}} + \delta U \exp(-\Theta^2/2.25) \ , \quad (7)$$

where Θ is the nuclear temperature (in MeV) and is related to the excitation energy E^* by the following statistical expression:[13]

$$\Theta = (10 E^*/A)^{1/2} \ . \quad (8)$$

Apparently, according to relation (7) the shell correction $\delta U(\Theta)$ decreases as the temperature increases, and for complete washing away of the shell effects the potential is given simply by the liquid drop model potential V_{LDM}. The mass parameters should also vary with temperature,[14] but no usable prescription is available to date.

Finally, for the dynamical mass fragmentation process, we quantize the motion in the mass asymmetry coordinate η. Considering that the η motion is fast compared to the R motion, R can be taken as a time-independent parameter and the stationary Schrödinger equation in η, using the Pauli-Padolsky prescription, can be written as[7]

$$\left[-\frac{\hbar^2}{2\sqrt{B_{\eta\eta}}} \frac{\partial}{\partial\eta} \frac{1}{\sqrt{B_{\eta\eta}}} \frac{\partial}{\partial\eta} + V(\eta) \right] \Psi_R^{(\nu)}(\eta) = E_R^{(\nu)} \Psi_R^{(\nu)}(\eta) \ . \quad (9)$$

We choose the value of constant R at a point just after the barrier penetration, under the assumption that the main behavior of the distributions is already fixed at this point. After the tunneling is completed (or the saddle is formed), the fissioning system simply runs down the barrier. This assumption is widely used[15-18] and is supported by the near constancy of the potentials $V(\eta)$ and fission mass yields (described below) at later stages of R (Refs. 7 and 15), and also by an explicit fission model calculation[19] involving the analytical solution of the time-dependent Schrödinger equation. More recently, the fragmentation theory is extended[20] to include the dynamical coupling of mass asymmetry η with the relative motion R, demonstrating explicitly that this coupling effect is of negligible order for the mass yields in α-particle transfer resonances. Furthermore, now an experimental verification of this assumption is also given,[21] at least for the nuclear charge, indicating that division of nuclear charge is decided much earlier than for neutrons, so that on the way to scission the two nascent fragments are polarized by the Coulomb repulsion and they are linked by a neutron rich neck. The present calculations, however, indicate some possible contribution of this coupling between R and η, though the main results of the experiments are still obtained within the above approximation.

Equation (9) is solved numerically. Then, $|\Psi_R(\eta)|^2$ gives the probability of finding the mass fragmentation η at the position R, which when scaled to mass yield Y (in percent) at the mass, say, A_1 of one fragment $(d\eta = 2/A)$, gives the mass distribution yield

$$Y(A_1) = |\Psi_R(\eta(A_1))|^2 \sqrt{B_{\eta\eta}(A_1)} \frac{200}{A/2} \ . \quad (10)$$

This yield is directly comparable with experiments. If only the ground state contributes and there is a complete adiabaticity, then $\nu = 0$. However, if the system is excited or we allow the effects of interaction with other degrees of freedom, then higher values of ν would contribute. The possible consequences of such excitations are also included here through the simple Boltzmann-like occupation of excited states.

$$|\Psi_R|^2 = \sum_{\nu=0}^{\infty} |\Psi_R^{(\nu)}|^2 \exp(-E_R^{(\nu)}/\Theta) \ . \quad (11)$$

III. ANGULAR MOMENTUM DEPENDENT ADIABATIC SCATTERING POTENTIALS

First of all, we argue about the possibility of this phenomena of fusion and subsequent fission in reactions of ^{208}Pb on various light targets, from the point of view of the amount of angular momentum l a fused system can carry. This is also used by Ngô et al.[22] for the "fast-fission" phenomena—a process whose characteristics are similar to those of fission following compound nucleus

formation. Figure 1 shows, as an illustrative example, the adiabatic scattering potentials for ^{208}Pb$+^{50}$Ti$\rightarrow^{258}$104, calculated for different angular momentum l values. Some of the associated nuclear shapes for this and other colliding systems are shown in Fig. 2 of paper I, and are used here for calculating the moment of inertia $\mathcal{I}_{\perp}$ in the rotational energy term V_l [Eqs. (3) and (A5)].

We first notice from Fig. 1 that the barrier exists for $l=0$ and the effective barrier height decreases as l increases. For some $l=l_{\mathrm{cr}}$, the barrier vanishes completely ($l_{\mathrm{cr}}=268$ for this system). Since the lowest incident bombarding energy used for this reaction is greater than the height of the Coulomb barrier, $E_{\mathrm{c.m.}}/V_C>1$ (see column 4 in Table 2 of Ref. 1), the incoming system gets captured in the pocket behind the barrier and forms a compound system. However, the incoming system being very asymmetric, the compound system is very much excited[3] (see also column 5 in Table 2 of Ref. 1) and fissions rather than proceeding to the ground state for forming a cool compound nucleus. The effective barrier against fission is apparently less as l increases. For $l\geq l_{\mathrm{cr}}$, since the barrier reduces to zero, we say that the probability of forming the
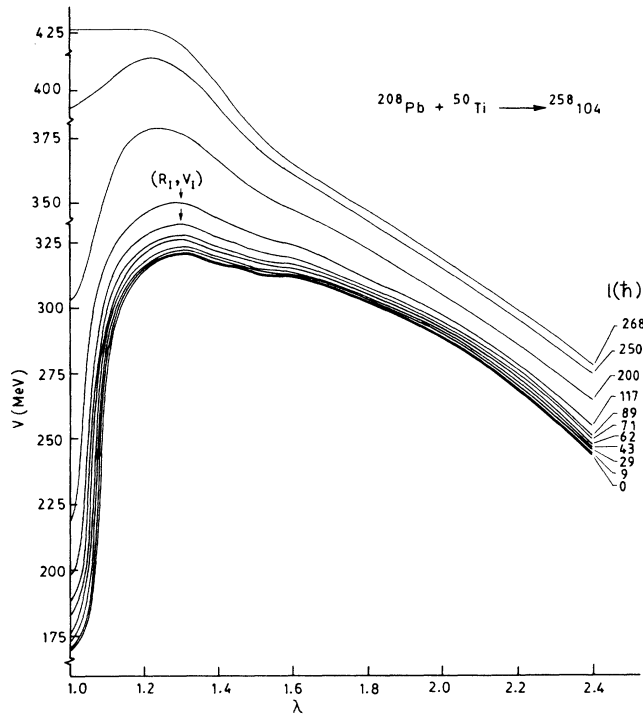

FIG. 1. The adiabatic scattering potentials for ^{208}Pb$+^{50}$Ti $\rightarrow^{258}$104, calculated for different angular momentum l values. The energy scale is normalized to the binding energy E_B ($=2074.25$ MeV) of ^{208}Pb$+^{50}$Ti at $R=\infty$. For the complete overlap of nuclei ($\lambda=1.0$), following earlier work (Ref. 23), the curves are extrapolated to the ground state binding energy $E_{\mathrm{g.s.}}$ of the compound system ($E_{\mathrm{g.s.}}+E_B=-1904.70+2074.25$ $=169.55$ MeV for $l=0$) with V_l added for a spherical compound nucleus. The choices of $0<l<l_{\mathrm{cr}}$ correspond to l_c values given in Table I.

TABLE I. Some of the characteristic quantities for the reactions with ^{208}Pb.

Reaction	E_{lab}/A (MeV/nucleon)	$E_{\mathrm{c.m.}}$ (MeV)	l_c ($\hbar$)	l_{cr} ($\hbar$)
^{208}Pb$+^{50}$Ti	4.77	192	9	
	5.00	202	29	
	5.25	211	43	
	5.50	222	62	
	5.90	238	71	
	6.50	263	89	
	8.00	323	117	
				268
^{208}Pb$+^{52}$Cr	5.24	218	21	
	5.50	228	41	
	5.90	245	57	
	6.50	270	79	
	8.00	332	102	
				300
^{208}Pb$+^{58}$Fe	5.24	238	15	
	5.50	249	34	
	5.90	268	50	
	6.50	295	79	
	8.00	363	107	
				<311[a]
^{208}Pb$+^{64}$Ni	5.24	256	3	
	5.50	269	13	
	5.90	289	42	
	6.50	319	65	
	8.00	392	107	
				<317[a]

[a]The ground state binding energies for these compound systems were not available. We have used here the corresponding values given in Seegre's table (Ref. 10) for ^{267}108 and ^{273}110.

compound system is zero. The l_{cr} values, for all the systems studied here, are calculated and given in Table I.

Next, since the capture cross sections σ_c are measured,[1] the angular momentum l_c carried by the compound system formed at each bombarding center-of-mass energy $E_{\mathrm{c.m.}}$ can be calculated by using the sharp cutoff approximation,

$$\sigma_c=\frac{\pi\hbar^2}{2\mu E_{\mathrm{c.m.}}}l_c^2 . \tag{12}$$

This means that at a given $E_{\mathrm{c.m.}}$ the compound system formed with cross section σ_c can carry an angular momentum l_c. These numbers are also given in Table I for all the reactions of ^{208}Pb on ^{50}Ti, ^{52}Cr, ^{58}Fe, and ^{64}Ni. The scattering potentials given in Fig. 1 are, for the l values, greater than or equal to these l_c values. As already observed, for each of $l=l_c$ the barrier exists for capturing the incoming nuclei to form the compound system and in each case the barrier is low enough for the compound system formed to be able to fission. This is exactly what has been observed in the experiments of Bock et al.[1] for the bombarding energies up to 8 MeV/nucleon.

Furthermore, we notice in Table I that the critical angular momentum l_{cr} for all these reactions corresponds to $E_{lab}/A \gg 8$ MeV/nucleon. Hence it will be of interest to see what happens beyond the present range of the experiments.[1] In the following sections, we analyze further these two steps of capture and subsequent fission more quantitatively.

IV. CAPTURE CROSS SECTIONS

For the first step of the model, we have calculated the capture cross sections by using the sharp cutoff model expression

$$\sigma_c = \pi R_I^2 (1 - V_I / E_{c.m.}) , \qquad (13)$$

where R_I and V_I are the positions and heights of the interaction barriers. We have seen in Fig. 1 that V_I varies considerably with incident energy (the l value) and R_I (l) remains constant ($R_I = 7.74$ fm for $^{208}Pb + ^{50}Ti$). In view of this result, for the calculations of σ_c as a function of $E_{c.m.}$, shown in Fig. 2, we have used (i) the barrier for $l = 0$ only (dashed lines), and (ii) the l-dependent barriers (solid lines). For comparisons, we have normalized the calculations to the experimental data[1] (shown as dots with error bars) at one point (the lowest $E_{c.m.}$ value). This is essential because the interaction (or fusion) barriers are known[24-26] to lie higher and at much smaller R values than the Coulomb barriers. We notice in Fig. 2 that our calculations show a reasonable agreement with experiments, particularly for the low energy region and for the angular momentum dependent interaction barriers.
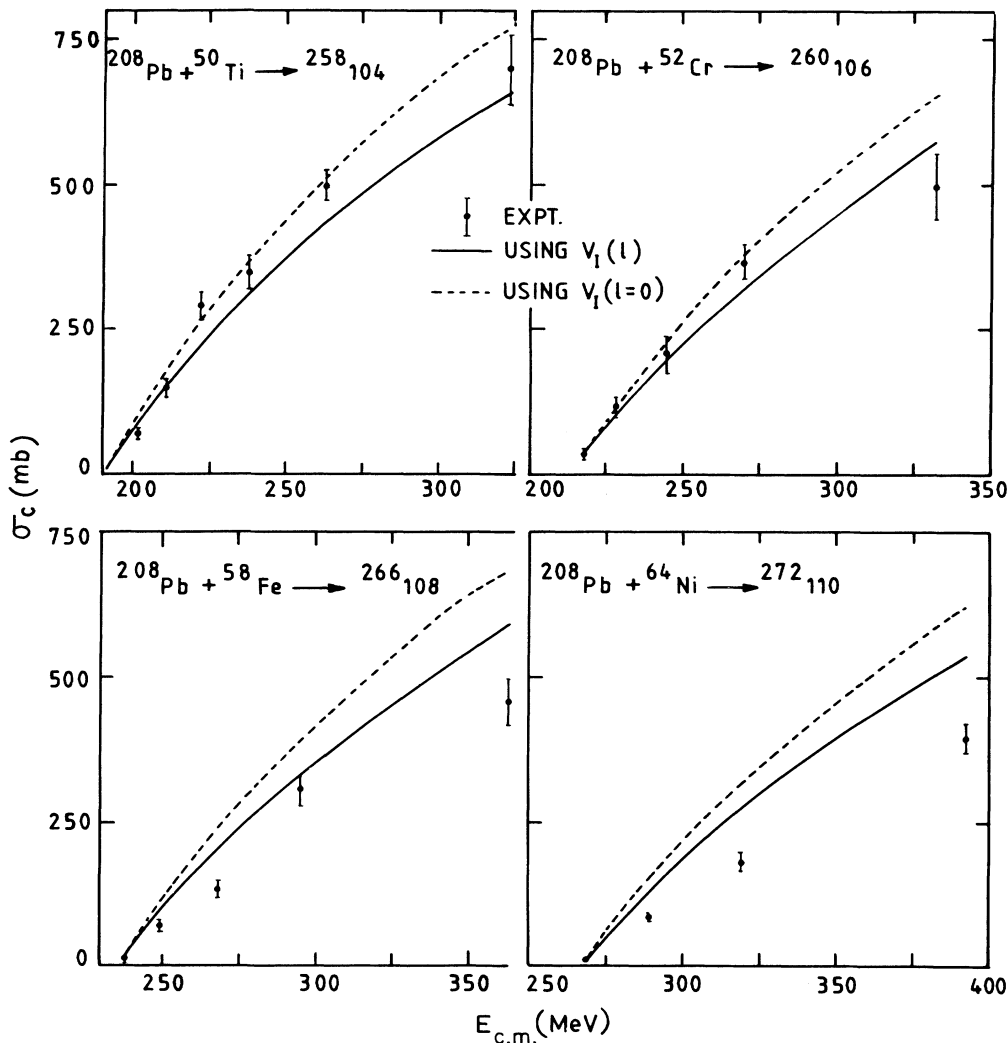

FIG. 2. The capture cross section σ_c as a function of the center-of-mass energy $E_{c.m.}$ Our calculations, in the sharp cutoff approximation, are made for a constant V_I ($l = 0$) (dashed lines) and for l-dependent V_I (solid lines) and compared with the experimental data of Bock et al. (Ref. 1) (dots with error bars).

V. MASS FRAGMENTATION DISTRIBUTION YIELDS

The second step of our model is to calculate the mass fragmentation distribution yields for the fission of the excited composite systems formed. Figures 3—6 show the calculated adiabatic fragmentation potentials $V(\eta)$ and the adiabatic cranking masses B_{ij} $(i,j=\eta,R)$ for all four composite systems $^{258}104^*$, $^{260}106^*$, $^{266}108^*$, and $^{272}110^*$, respectively. In view of the discussion following Eq. (9), the λ value is chosen near the top of the barrier and the effect of varying this choice is then studied. We notice in Figs. 3—6 that in each case the liquid drop potential $V_{LDM}(\eta)$ is smooth, like a simple harmonic oscillator, and the shell effects δU contribute to both the potential and mass parameters. The effect of temperature Θ on the potential, given by Eq. (7), is shown in Fig. 3 for the illustrative case of $^{258}104$. We notice that the shell effects $\delta U(\Theta)$ reduce as Θ increases and for $\Theta=1.90$ MeV, which corresponds to 6.5 MeV/nucleon for ^{208}Pb bom-

barded on ^{50}Ti, the shell effects are nearly zero such that the total potential $V(\eta)$ reduces almost to $V_{LDM}(\eta)$. Similar effects are expected for the mass parameters, but, as stated above, to date one does not know how to calculate the mass parameters at finite temperatures.

The mass fragmentation yields, calculated by using the potentials $V_{LDM}+\delta U(\Theta)$ and the masses $B_{\eta\eta}$ of Figs. 3—6 at various Θ values corresponding to the available experimental data,[1] are presented in Figs. 7—10, respectively, for fission of $^{258}104$, $^{260}106$, $^{266}108$, and $^{272}110$. The temperature effects are also included by allowing, through Eq. (11), the fission from excited states. The experimental data, shown as dots, are derived from Fig. 10 of Ref. 1 at the three incident energies of 5.5, 5.9, and 6.5 MeV/nucleon. The data at 5.2 MeV/nucleon are not considered here because they are similar to those at 5.5 MeV/nucleon and are less precise. It is also relevant to mention here that the data on the shoulders at lower energies, i.e., the peaks at $A_2\approx200$ and $A_1=A-A_2$, seen in the experiments, are not certain[1] because the measurements are unreliable for $\eta>0.4$. In other words, experimentally only the symmetric fragmentation can be said to be seen at all the incident energies.[1] In the following
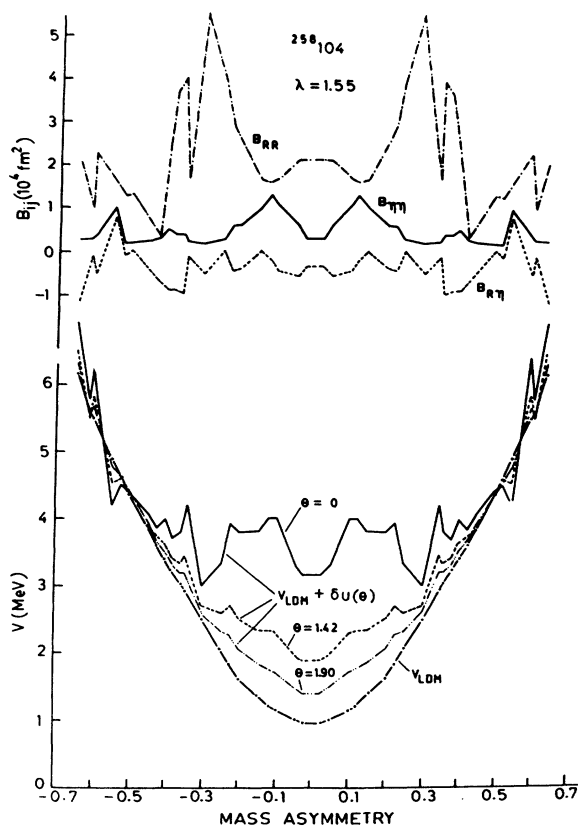

FIG. 3. The adiabatic (a) fragmentation potentials and (b) cranking mass parameters (in units of the nucleon mass m) for the compound system $^{258}104$ at $\lambda=1.55$. In (a) the dotted-dashed curve gives the liquid drop model potential V_{LDM} (calculated for 24 points that are shown as dots) and the solid line gives the total potential [$V_{LDM}+\delta U(\Theta=0)$]. The other two curves illustrate the effect of temperature Θ on the shell corrections δU.
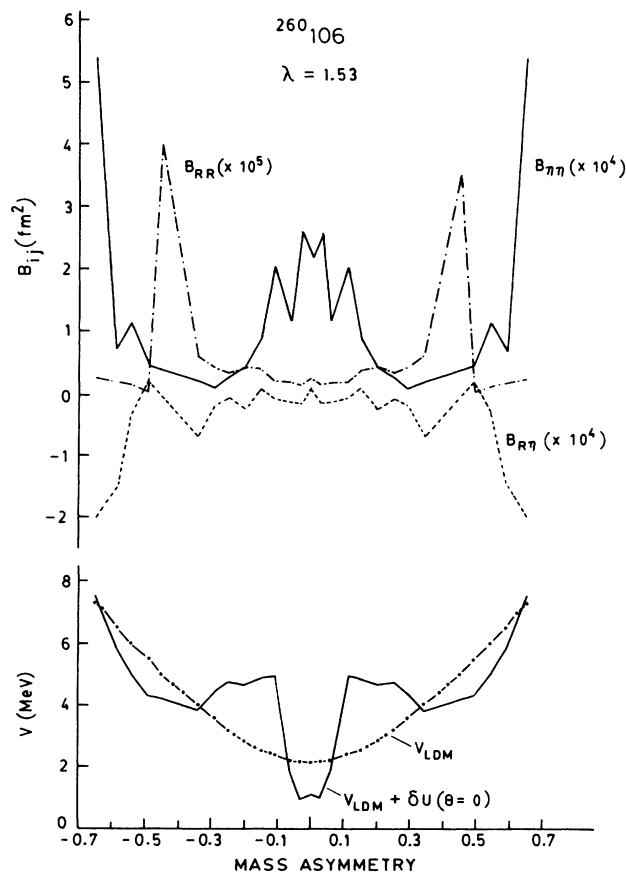

FIG. 4. Same as in Fig. 3, except for the compound system $^{260}106$ at $\lambda=1.53$.

paragraph we shall see that this result might have an important consequence for the dynamical fragmentation process. We shall first analyze the case of $^{258}104$ (refer to Fig. 7) in detail and then give our results for other systems.

Figure 7(a) refers to the calculations and the experimental data at $E_{c.m.} = 5.5$ MeV/nucleon ($\Theta = 1.42$ MeV) for the composite system $^{258}104$. Curve 1 gives the results of our calculation for $V_{LDM} + \delta U(\Theta = 1.42$ MeV$)$ and $B_{\eta\eta}(\eta)$. We notice here strong peaks at $A_2 = 199$ and $A_1 = 59$ and some other structure. The interesting point about this structure as well as the peaking effect is that, except for the decrease or increase of amplitudes, no change occurs when $\delta U = 0$, i.e., only V_{LDM} is used (curve 1') or $\Theta = 0$, i.e., no temperature dependence at all (curve 1''). Apparently, then, both the peaks and other structure in the distribution are not due to shell effects in the potential. In order to study the role of large structure in mass parameters $B_{\eta\eta}(\eta)$, which might get reduced with the addition of temperature in it, we have calculated the mass yields using the averaged constant mass $\overline{B}_{\eta\eta}$ ($= 5 \times 10^3$ fm^2, in units of nucleon mass, for the present case of $^{258}104$ at $\lambda = 1.55$). This is shown by curves 2 and 2' calculated, respectively, for $V_{LDM} + \delta U(\Theta = 1.42$ MeV$)$ and V_{LDM} alone. We notice that these two distributions are identical and completely smooth, without any peaking ef-

fect [curve 2 is slightly broader because of the additional $\delta U(\Theta = 1.42$ MeV$)$ energy]. Thus, it seems that the peaking effect as well as the other structure in the distributions arose due to the large structure in masses $B_{\eta\eta}(\eta)$. A realistic temperature dependence on masses, however, might not be able to keep this result and one has to then look for their source somewhere else. Figures 7(b) and 7(c), referring to $E_{c.m.} = 5.9$ and 6.5 MeV/nucleon or $\Theta = 1.62$ and 1.90 MeV, respectively, give exactly the same results. Now, comparing our calculations with experiments, we notice that, if the shoulders or peaks observed in the experimental data are disregarded,[1] the symmetric mass fragmentation is simply the (dynamical) liquid drop effect. The calculated mass distributions are symmetric for the averaged constant mass parameter and with or without shell effects in the potential energy, thereby reproducing successfully the gross features of the experimental data.[1] With the increase of temperature, though, our calculated distributions do become broader, but not as much as is required by the experiments. The shoulders
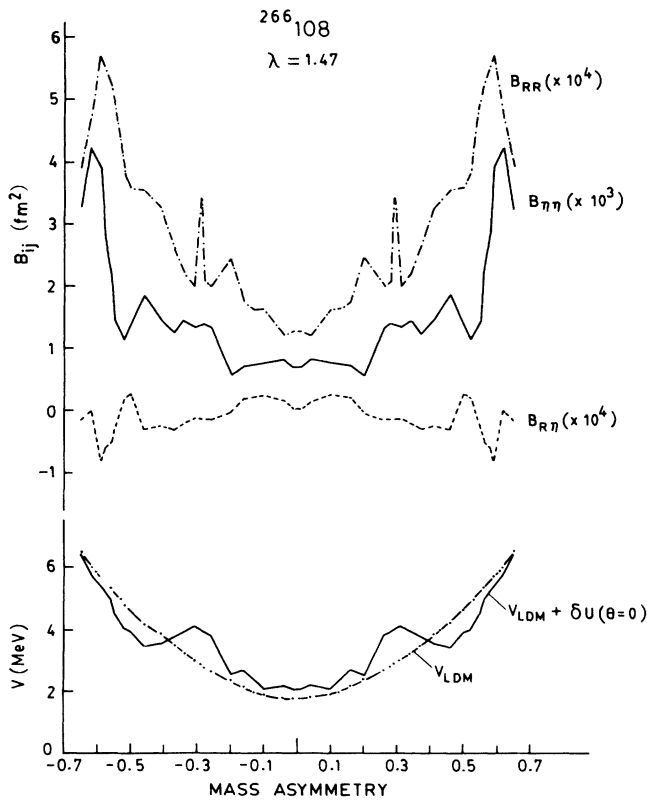

FIG. 5. Same as in Fig. 3, except for the compound system $^{266}108$ at $\lambda = 1.47$.
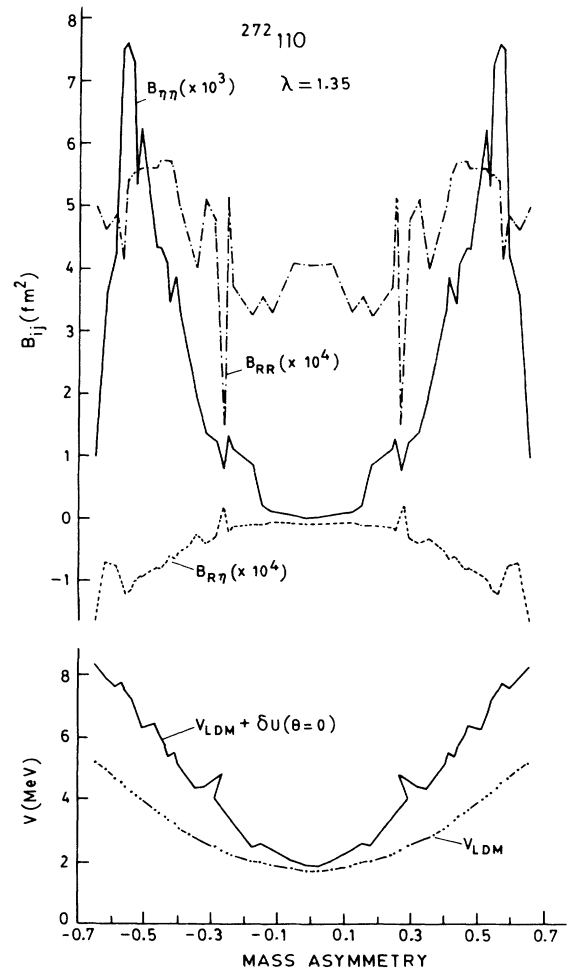

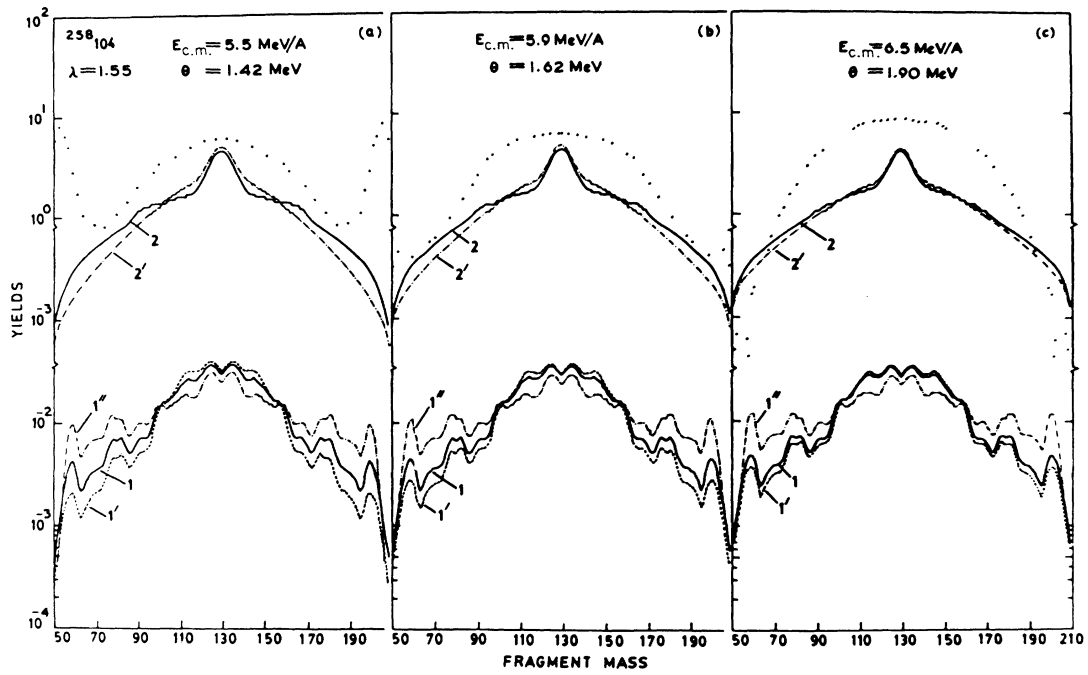FIG. 6. Same as in Fig. 3, except for the compound system $^{272}110$ at $\lambda = 1.35$.

FIG. 7. The calculated mass yield distributions compared with the experimental data, for the composite system ^{258}104 at $\lambda = 1.55$ and different temperatures (Θ values) or incident energies. Curves 1, 1', and 1'' give the calculated yields by using, respectively, the potentials $V_{LDM} + \delta U(\Theta)$, V_{LDM} or $V_{LDM} + \delta U(\Theta = 0)$, and $B_{\eta\eta}(\eta)$. Curves 2 and 2' give the calculated yields, respectively, for $V_{LDM} + \delta U(\Theta)$ or V_{LDM} and the average constant $\overline{B}_{\eta\eta} = 5 \times 10^3$ m fm^2. The experimental data, deduced from Fig. 10 of Ref. 1 at different incident energies, are shown as dots. The calculations are not normalized to experimental data.
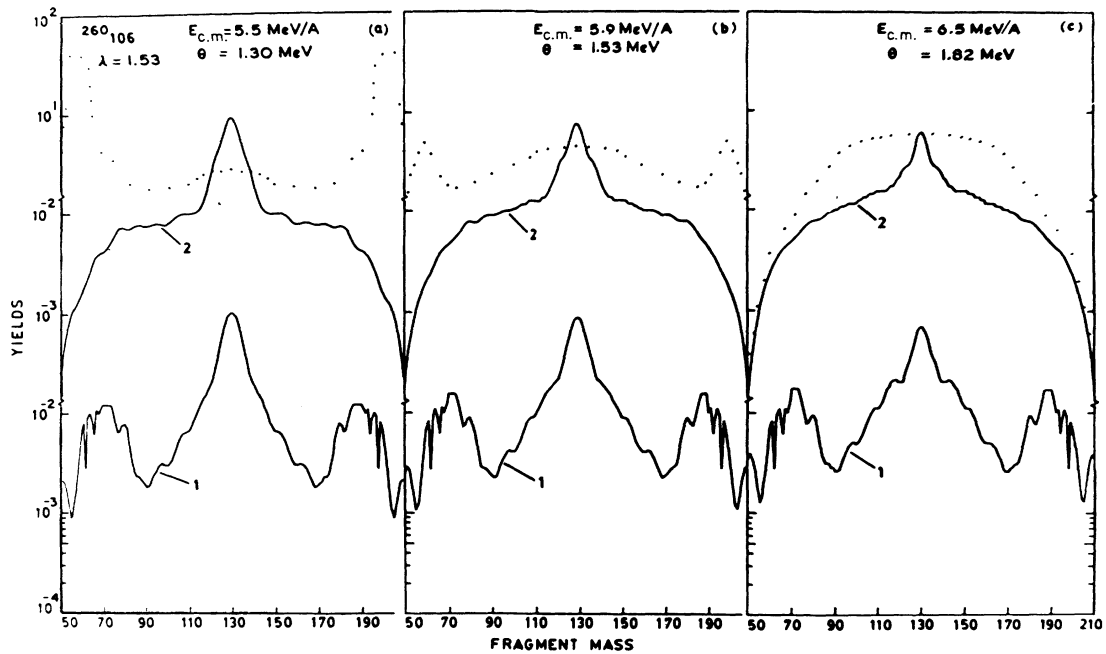
FIG. 8. Same as in Fig. 7, except for the compound system ^{260}106 at $\lambda = 1.53$ and $\overline{B}_{\eta\eta} = 2.2 \times 10^4$ m fm^2.
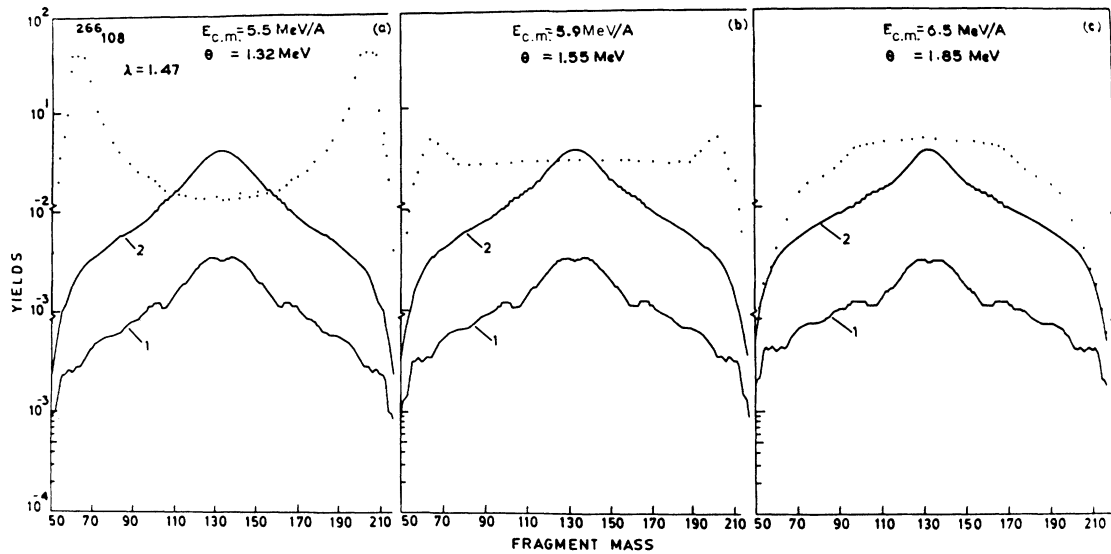
FIG. 9. Same as in Fig. 7, except for the compound system $^{266}108$ at $\lambda = 1.47$ and $\overline{B}_{\eta\eta} = 1.7 \times 10^3$ m fm^2.

are also predicted in our calculations, at about the same positions as observed in the present data,[1] and their absence, if confirmed, could help determine the effective dynamical role of the mass parameters. This demands, however, the use of temperature-dependent cranking masses.

In view of our observations in the last paragraph above, Figs. 8, 9, and 10 give for the systems $^{260}106$, $^{266}108$, and $^{272}110$, respectively, a comparison of the experimental data with calculated mass distribution yields for only two cases of $V_{LDM} + \delta U(\Theta)$ with (i) $B_{\eta\eta}(\eta)$ and (ii) constant $\overline{B}_{\eta\eta}$ (curves 1 and 2). Apparently, all the results obtained
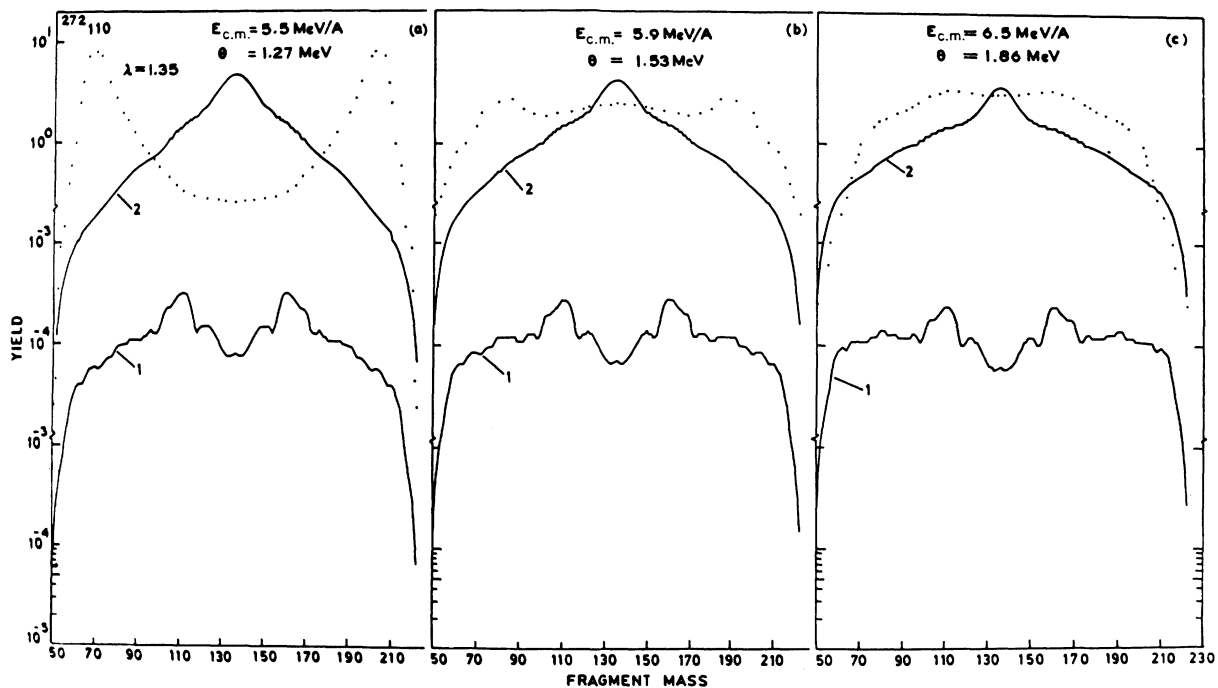
FIG. 10. Same as in Fig. 7, except for the compound system $^{272}110$ at $\lambda = 1.35$ and $\overline{B}_{\eta\eta} = 3 \times 10^3$ m fm^2.
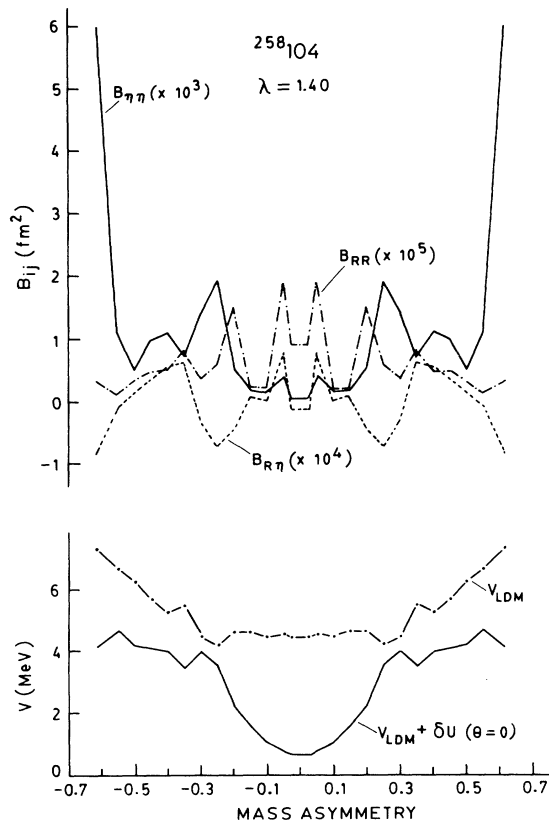
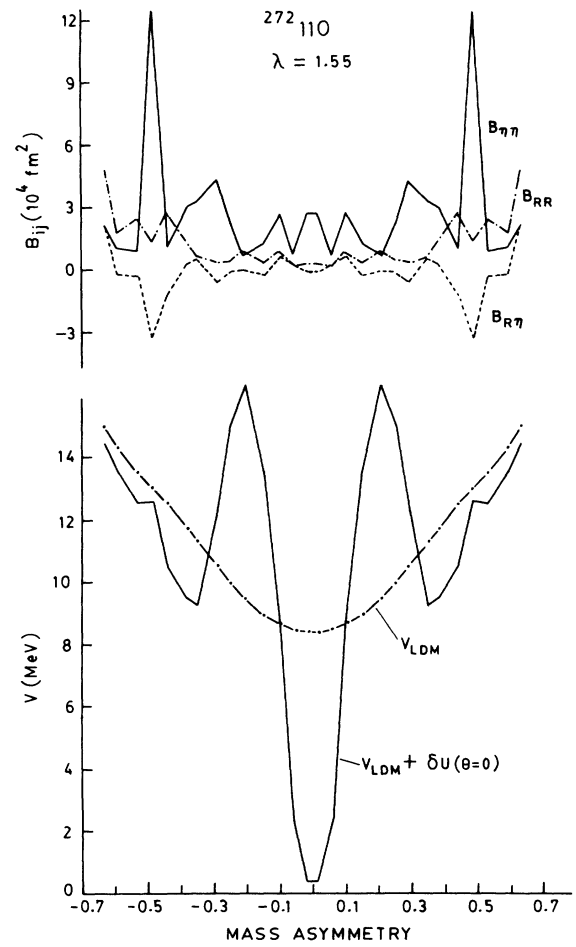FIG. 11. Same as in Fig. 3, except at $\lambda = 1.40$.
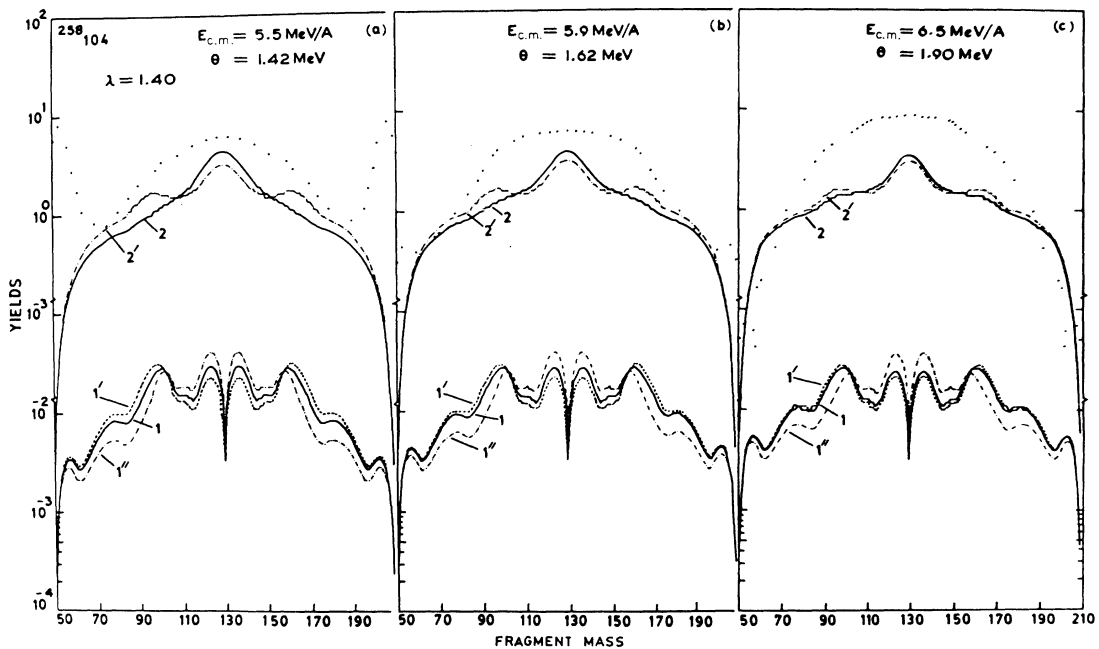
FIG. 12. Same as in Fig. 6, except at $\lambda = 1.55$.

FIG. 13. Same as in Fig. 7, except at $\lambda = 1.40$ and $\overline{B}_{\eta\eta} = 2.4 \times 10^3$ m fm^2.

above for $^{258}104$ are supported, except that no shoulders are predicted for $^{266}108$ and $^{272}110$. There is, however, still enough structure in the calculated distributions of $^{266}108$ and $^{272}110$ also, not present in experimental data, which is sensitive to the details of the mass parameters used.

Finally, in order to study the effect of varying the chosen λ value, we have shown in Figs. 11 and 12 the calculated potential and mass parameters for a choice of a smaller and a larger λ value, respectively, for the composite systems $^{258}104$ and $^{272}110$. The corresponding calculated yields are presented in Figs. 13 and 14. We notice that, in conformity with our earlier calculations,[15−19] the main results of the last two paragraphs are still obtained independent of the choice of λ value. The distributions are again symmetric. The important point of difference, however, lies in the predictions of detailed structure and shoulders. The shoulders now disappear in $^{258}104$, but are predicted in $^{272}110$. Thus, the question of shoulders, etc. in experimental data points out not only the problem of temperature dependence of mass parameters but also the dynamical coupling between relative motion and mass asymmetry for these reactions. This apparently calls for further experiments with refined measurements in the region of mass asymmetry $\eta > 0.4$.

VI. CONCLUSIONS

As an application of the "fusion model" of paper I, we have seen that in the reactions of 4.8—8 MeV/nucleon ^{208}Pb on ^{50}Ti, ^{52}Cr, ^{58}Fe, and ^{64}Ni, the colliding systems overcome the adiabatic interaction (or fusion) barriers and get captured in the pockets behind the barriers and form composite systems $^{258}104$, $^{260}106$, $^{266}108$, and $^{272}110$, respectively. Being strongly asymmetric systems, the excitation energies of the composite systems formed are large, so that they fission back adiabatically. The fusion (or capture) cross sections are shown to compare reasonably well with experiments up to 8 MeV/nucleon and the gross features of the mass yields, i.e., the symmetric mass fragmentation are reproduced systematically, independent of the choice of relative separation distance R and the detailed structure in the cranking mass parameters. The symmetric fission is shown to be the (dynamical) liquid drop effect and the other detailed structures in the mass distributions, including the shoulders, are found to depend on (i) how the temperature would effect the variation of masses with mass asymmetry, and (ii) the dynamical coupling of mass asymmetry with the relative motion of the separating systems in these reactions. Therefore, refined measurements of the data for larger mass asymmetry ($\eta > 0.4$) are of great importance. The calculations of the
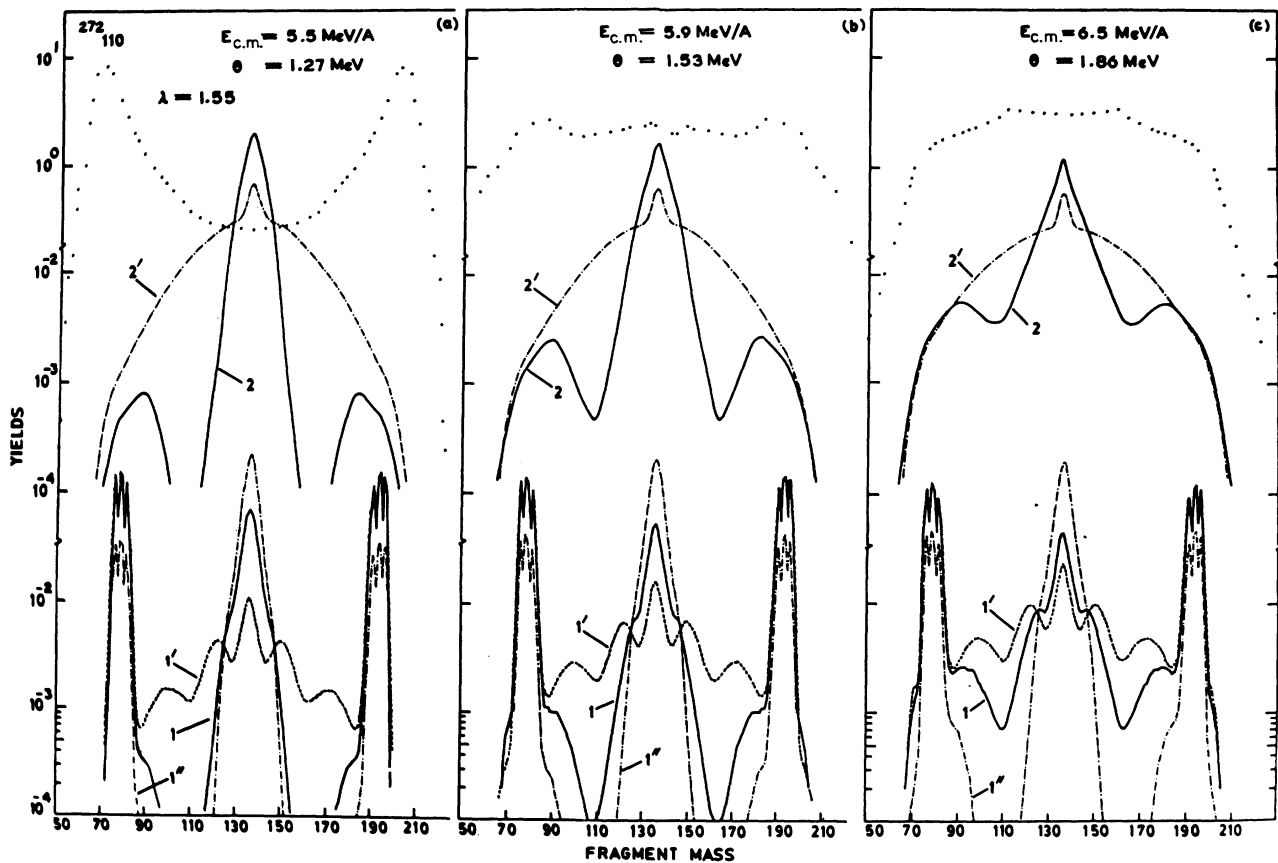

FIG. 14. Same as in Fig. 10, except at $\lambda = 1.55$ and $\overline{B}_{\eta\eta} = 2.8 \times 10^4$ m fm^2.

critical angular momentum for the vanishing of the fusion barrier also suggest extension of the present experiments to still higher energies.

Hence, in these reactions a two step process of "symmetric fragmentation following capture," which is given by the dynamical fragmentation theory, is clearly prevelent.
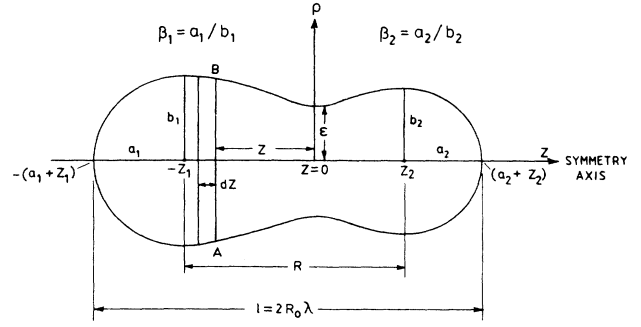
ACKNOWLEDGMENTS

FIG. 15. A typical nuclear shape obtained in the asymmetric two center shell model. The relevant geometry and other parameters are also indicated.

APPENDIX: MOMENT OF INERTIA FOR AN ASYMMETRIC TWO-CENTER SHELL MODEL NUCLEAR SHAPE

A typical nuclear shape obtained in the ATCSM is shown in Fig. 15. The generating function $\rho(Z)$ for such a shape is given by[8]

$$\rho^2(Z) = \begin{cases} \dfrac{1}{\beta_i^2}[a_i^2 - (Z-Z_i)^2] & \text{for } |Z| > |Z_i|, \\[4mm] \dfrac{1}{\beta_i^2} \dfrac{\{a_i^2 - \epsilon(Z-Z_i)^2[1+c'(Z-Z_i)+d'(Z-Z_i)^2]\}}{[1+g_i(Z-Z_i)^2]} & \text{for } |Z| < |Z_i| \end{cases} \tag{A1}$$

$(i=1,2)$, where the coefficients g_i are introduced to avoid the cusp in the potential and the factor $[1+c'(Z-Z_i)+d'(Z-Z_i)^2]$ allows for the variable barrier heights via the neck parameter ϵ.

We first consider that the nuclear system rotates about the axis ρ, perpendicular to the symmetry axis. For this purpose we take an infinitesimal disk of thickness dZ at a distance $|Z|$ from the origin. The moment of inertia of this infinitesimal disk about its diameter AB is

$$\mathscr{I}_{AB} = \tfrac{1}{4}\sigma\pi\rho^2(Z)dZ\,\rho^2(Z) = \tfrac{1}{4}\pi\sigma\rho^4(Z)dZ \ , \tag{A2}$$

where $\sigma = M/[(4\pi/3)R_0^3]$ is the nuclear density of an equivalent spherical nucleus of radius R_0 and mass $M = Am$, m being the nucleon mass. Then, using the parallel axis theorem $(\mathscr{I}_\rho = \mathscr{I}_{AB} + MZ^2)$ and integrating over the limits of variation of Z, the moment of inertia of the total system about the axis ρ, perpendicular to the symmetry axis, is given by

$$\mathscr{I}_\perp = \mathscr{I}_\rho = \tfrac{1}{4}\pi\sigma \int_{-(a_1+Z_1)}^{(a_2+Z_2)} \rho^4(Z)dZ + \pi\sigma \int_{-(a_1+Z_1)}^{(a_2+Z_2)} \rho^2(Z)Z^2 dZ \ . \tag{A3}$$

This integral can be solved by substituting for $\rho(Z)$ from (A1) and by noting that

$$\begin{aligned} \int_{-(a_1+Z_1)}^{(a_2+Z_2)} f(Z)dZ &= \int_{-(a_1+Z_1)}^{-Z_1} f(Z)dZ + \int_{-Z_1}^{0} f(Z)dZ + \int_{0}^{Z_2} f(Z)dZ + \int_{Z_2}^{(a_2+Z_2)} f(Z)dZ \\ &= -\left[\int_{(a_1+Z_1)}^{Z_1} f(Z)dZ + \int_{Z_1}^{0} f(Z)dZ \right] + \int_{0}^{Z_2} f(Z)dZ + \int_{Z_2}^{(a_2+Z_2)} f(Z)dZ \\ &= \int_{0}^{Z_1} f(Z)dZ + \int_{Z_1}^{(a_1+Z_1)} f(Z)dZ + \int_{0}^{Z_2} f(Z)dZ + \int_{Z_2}^{(a_2+Z_2)} f(Z)dZ \ . \end{aligned} \tag{A4}$$

For the simple case of $c'=d'=0$, we get

$$\mathscr{I}_\perp = \frac{3Am}{4R_0^3}\left[\sum_{i=1}^2 \frac{1}{\beta_i^2}\left\{\frac{Z_i}{4\beta_i^2(1+g_iZ_i^2)}\left[\tfrac{1}{2}a_i^4+\frac{\epsilon a_i^2}{g_i}+\frac{\epsilon^2}{2g_i^2}\right]\right.\right.$$

$$+\frac{\tan^{-1}\sqrt{g_i}Z_i}{8\sqrt{g_i}}\left[\frac{a_i^4}{\beta_i^2}-\frac{2\epsilon a_i^2}{\beta_i^2 g_i}-\frac{8a_i^2}{g_i}+8Z_i^2a_i^2-\frac{3\epsilon^2}{\beta_i^2 g_i^2}-\frac{8\epsilon}{g_i^2}+\frac{8\epsilon Z_i^2}{g_i}\right]$$

$$-\frac{Z_i(g_ia_i^2-\epsilon)}{g_i^2}\ln(1+g_iZ_i^2)+\left[\frac{2a_i^5}{15\beta_i^2}-\tfrac{1}{30}(a_i+Z_i)^5+\tfrac{1}{6}a_i(a_i+Z_i)^4-\tfrac{1}{3}a_i^2Z_i^3\right.$$

$$\left.\left.\left.+\frac{Z_ia_i^2}{g_i}-\frac{7\epsilon Z_i^3}{3g_i}+\frac{\epsilon Z_i}{g_i^2}+\frac{\epsilon^2 Z_i}{4\beta_i^2 g_i^2}+\tfrac{1}{30}Z_i^5\right]\right\}\right]. \tag{A5}$$

Similarly, using the perpendicular axis theorem $(\mathscr{I}_Z=2\mathscr{I}_{AB})$, the moment of inertia of a nucleus of shape given by Fig. 15, about the symmetry axis, is given by (for $c'=d'=0$)

$$\mathscr{I}_\parallel=\mathscr{I}_Z=\tfrac{1}{2}\pi\sigma\int_{-(a_1+Z_1)}^{(a_2+Z_2)}\rho^4(Z)dZ=\frac{3Am}{8R_0^3}\left\{\sum_{i=1}^2\frac{1}{\beta_i^4}\left[\frac{Z_i}{(1+g_iZ_i^2)}\left[\tfrac{1}{2}a_i^4+\frac{\epsilon a_i^2}{g_i}+\frac{\epsilon^2}{2g_i^2}\right]\right.\right.$$

$$\left.\left.+\frac{1}{\sqrt{g_i}}\tan^{-1}\sqrt{g_i}Z_i\left[\tfrac{1}{2}a_i^4-\frac{\epsilon a_i^2}{g_i}-\frac{3\epsilon_i^2}{2g_i^2}\right]+\frac{\epsilon^2 Z_i}{g_i^2}+\frac{8a_i^5}{15}\right]\right\}. \tag{A6}$$

As a corollary, one can show that, for an ellipsoidal nucleus $(Z_1=Z_2=0,\quad c'=d'=g_1=g_2=0,\quad \epsilon=1,\quad$ and $a_1=a_2=a$ and $\beta_1=\beta_2=\beta)$,

$$\rho^2(Z)=\frac{1}{\beta^2}(a^2-Z^2), \tag{A7}$$

and

$$\mathscr{I}_\perp=\frac{1}{5}\frac{Ama^5}{R_0^3\beta^2}\left[1+\frac{1}{\beta^2}\right], \tag{A8}$$

$$\mathscr{I}_\parallel=\frac{2}{5}\frac{Ama^5}{R_0^3\beta^4}. \tag{A9}$$

Finally, for a sphere $(\beta=1, a=R_0)$, we get from (A8) and (A9) the well known result

$$\mathscr{I}_\perp=\mathscr{I}_\parallel=\tfrac{2}{5}AmR_0^2. \tag{A10}$$

[1] R. Bock, Y. T. Chu, M. Dakowski, A. Gobbi, E. Grosse, A. Olmi, H. Sann, D. Schwalm, U. Lynen, W. Müller, S. Bjornholm, H. Esbensen, W. Wölfi, and E. Morenzoni, Nucl. Phys. A388, 334 (1982).

[2] See, e.g., J. V. Kratz, A. E. Norris, and G. T. Seaborg, Phys. Rev. Lett. 33, 502 (1974).

[3] N. Malhotra, R. Aroumougame, D. R. Saroha, and R. K. Gupta, Phys. Rev. C 33, 156 (1986).

[4] H. Stöcker, R. Y. Cusson, H. J. Lustig, A. Gobbi, J. Hahn, J. A. Maruhn, and W. Greiner, Z. Phys. A 306, 235 (1982).

[5] W. J. Swiatecki, Nucl. Phys. A376, 275 (1982).

[6] R. K. Gupta, Z. Phys. A 281, 159 (1977).

[7] See, e.g., the following reviews: H. J. Fink, W. Greiner, R. K. Gupta, S. Liran, H. J. Maruhn, W. Scheid, and O. Zohni, in Proceedings of the International Conference on Reactions Between Complex Nuclei, Nashville, 1974 edited by R. L. Robinson, F. F. McGowan, J. B. Ball, and J. H. Hamilton (North-Holland, Amsterdam, 1975), Vol. 2, p. 21; R. K. Gupta, Fiz. Elem. Chastits At. Yad. 8, 717 (1977) [Sov. J. Part. Nucl. 8, 289 (1977)]; J. A. Maruhn, W. Greiner, and W. Scheid, in Heavy Ion Collisions, edited by R. Bock (North-Holland, Amsterdam, 1980), Vol. 2, Chap. 6; R. K. Gupta, D. R. Saroha, and N. Malhotra, J. Phys. (Paris) Colloq. 45, C6-477 (1984).

[8] J. Maruhn and W. Greiner, Z. Phys. 251, 431 (1972).

[9] W. D. Myers and W. J. Swiatecki, Ark. Fiz. 36, 343 (1967).

[10] P. A. Seeger, Nucl. Phys. A238, 491 (1975).

[11] D. R. Inglis, Phys. Rev. 96, 1059 (1959); S. T. Balyaev, Kgl. Dansk. Vidensk. Sels. Mat.-Fys. Medd. 31, No. 11 (1959).

[12] A. S. Jensen and J. Damgaard, Nucl. Phys. A203, 578 (1973).

[13] K. J. Le Cauteur and W. D. Lang, Nucl. Phys. 13, 32 (1959).

[14] A. Iwamoto and W. Greiner, Z. Phys. A 292, 301 (1979); A. Iwamoto and J. A. Maruhn, ibid. 293, 315 (1979).

[15] J. Maruhn and W. Greiner, Phys. Rev. Lett. 32, 548 (1974).

[16] R. K. Gupta, W. Scheid, and W. Greiner, Phys. Rev. Lett. 35, 353 (1975).

[17] D. R. Saroha and R. K. Gupta, Phys. Rev. C 29, 1101 (1984).

[18] R. K. Gupta and D. R. Saroha, Phys. Rev. C 30, 395 (1984).

[19] D. R. Saroha, R. Aroumougame, and R. K. Gupta, Phys. Rev. C 27, 2720 (1983).

[20] S. S. Malik, N. Malhotra, D. R. Saroha, and R. K. Gupta, International Centre for Theoretical Physics, Trieste, Italy, Internal Report No. IC/86/128.

[21] F. Caitucoli, M. Asghar, G. Barreau, B. Leroux, P. Perrin, M. Maurel, T. P. Doan, and A. Sicre, in Proceedings of the International Conference on Nuclear Data for Basic and Applied Science, Sante Fe, 1985 (unpublished).

[22] C. Ngô, C. Gregoire, and B. Remand, in Dynamics of Heavy

Ion Collisions (3rd Adriatic Europhysics Study Conference, Hvar, Yugoslavia, 1981), edited by N. Cindro, R. A. Ricci, and W. Greiner (North-Holland, Amsterdam, 1981).

[23]M. Münchow, D. Hahn, and W. Scheid, Nucl. Phys. **A388**, 381 (1982); N. Malhotra and R. K. Gupta, Phys. Rev. C **31**, 1179 (1985).

[24]H. H. Gutbrod, W. G. Winn, and M. Blann, Phys. Rev. Lett. **30**, 1259 (1973).

[25]H. H. Gutbrod, W. G. Winn, and M. Blann, Nucl. Phys. **A213**, 267 (1973).

[26]R. K. Gupta, A. Săndulescu, and W. Greiner, Phys. Lett. **67B**, 257 (1977).